Water Resources Research

RESEARCH ARTICLE
10.1029/2018WR024326

An Intercomparison of Noah Model Skills With Benefits of Assimilating SMOPS Blended and Individual Soil Moisture Retrievals

Jifu Yin[1,2], **Xiwu Zhan**[2], **Jicheng Liu**[1,2], **and Mitch Schull**[1,2]

[1]ESSIC/CICS, University of Maryland College Park, College Park, MD, USA, [2]NOAA NESDIS Center for Satellite Applications and Research, College Park, MD, USA

Key Points:
- Blended and individual microwave satellite soil moisture data were intercompared
- Benefits of assimilating blended and individual soil moisture retrievals are evaluated
- Results may help soil moisture data users choose data products from SMOPS

Correspondence to:
J. Yin,
jyin@umd.edu

Citation:
Yin, J., Zhan, X., Liu, J., & Schull, M. (2019). An intercomparison of Noah model skills with benefits of assimilating SMOPS blended and individual soil moisture retrievals. *Water Resources Research*, *55*, 2572–2592. https://doi.org/10.1029/2018WR024326

Received 29 OCT 2018
Accepted 3 JAN 2019
Accepted article online 8 JAN 2019
Published online 2 APR 2019

Abstract Soil moisture (SM) data from Soil Moisture Operational Product System (SMOPS) have been available and used by users since 2013, and the latest version (3.0) has been operationally released since 2017. The version 3.0 provides a combination of currently all available daily global microwave SM retrievals including observations of ASCATA, ASCATB, SMAP, SMOS, and AMSR2 from 1 April 2015 to present. This study intercompares Noah model skills with benefits of assimilating the SMOPS blended (hereafter, SMOPS) and the five individual satellite SM retrievals. Results show that SMOPS SM product presents a significant advantage in data availability in comparison with the individual SM retrievals. Significant differences in data availability, climatology, and dynamic range of SM values between the bias-corrected SMOPS and individual SM data lead to remarkable distinctions in Noah model SM simulations. Significant improvements of assimilating individual and blended satellite SM retrievals on model SM simulations versus the open loop in both surface and root zone soil layers are evident with reducing the Soil Climate Analysis Network measurements-based root mean square errors and raising the correlations with respect to the enhanced vegetation index. Compared to the individual SM assimilations, model SM estimations with benefits of assimilating the SMOPS data provide the more remarkable improvements in surface soil layer.

1. Introduction

Soil moisture (SM) plays a key role in the terrestrial water cycle (Rodriguez-Iturbe et al., 1999) and significantly impacts land-atmosphere water, energy, and carbon exchanges (Yin et al., 2014). At a continental scale, the positive feedback of SM precipitation is a significant rainfall source (Koster et al., 2004; van der Schrier & Barkmeijer, 2007), and thus, precipitation is generally decreased under a lack SM condition. Meanwhile, SM controls precipitation-runoff response at a watershed scale, especially where saturation surplus runoff processes dominate (Robinson et al., 2008). Through altering soil physical properties, soil biogeochemistry, and hierarchy of physiological responses in plants, SM is an important variable in affecting plant growth (Schwinning et al., 2004; Turcu et al., 2005). As such, SM constrains plant transpiration and photosynthesis, as well as biogeochemical cycles (Seneviratne et al., 2010). Accurate knowledge of the SM status would thus serve as good land surface initializations in coupled numerical weather prediction systems and climate models for improved weather, hydrological, and climatological predictions (Koster et al., 2004). Additionally, SM can also be used to monitor and predict drought and flood development (Brocca et al., 2017); because a short of SM projects the high likelihood of a drought event and an excess of SM signifies a flood occurrence.

Traditional in situ observations provide reasonable SM assessments, but they lack sufficient coverage and consistency at regional and global scales. In contrast, land surface models (LSMs) may provide spatially and temporally consistent estimates and are thus implemented to track SM status (Crow et al., 2012). These LSMs are severely influenced by a large number of vegetation and soil state parameters that are hard to specify for fine spatial resolutions at continental scales (Chen & Dudhia, 2001). These suboptimal model parameters result in errors of model outputs. Additionally, LSM simulations are also prone to errors from the uncertainties existing in the forcing data and the lack of scientific understanding in model physics (Mazrooei et al., 2015; Peters-Lidard et al., 2008; Reichle & Koster, 2004).

Meanwhile, recent microwave-based products (based on C- and X-band microwave observations) have included retrieving SM from satellite-based sensors, such as the Advanced Microwave Scanning Radiometer for Earth Observing System (AMSR-E) onboard Aqua (Njoku et al., 2003), the Advanced

Scatterometer (ASCAT) from both MetOp (Meteorological Operational Platform)-A and MetOp-B satellites (Wagner et al., 2013), AMSR2 onboard the Global Change Observation Mission-Water (GCOM-W) satellite (JAXA, 2013; Maeda et al., 2016), and WindSat (Li et al., 2010). Additionally, two more recent sensors have been designed to sense SM based on L-band microwave observations, including the Soil Moisture and Ocean Salinity (SMOS) satellite of the European Space Agency (ESA; Kerr et al., 2010) and National Aeronautics and Space Administration's Soil Moisture Active Passive (SMAP) (Entekhabi et al., 2010). However, these individual SM retrievals vary significantly from each other and lack complete coverages in space and time (Yin, Zhan, Zheng, Liu, et al., 2015). The ESA thus started to operationally release its Climate Change Initiative-blended SM product that combines various single-sensor active and passive microwave SM products in 2012 in support of climate research (Dorigo et al., 2017; Liu et al., 2016). To the certain time period, ESA Climate Change Initiative can provide the historical SM records. Meanwhile, to provide global satellite SM data products for National Oceanic and Atmospheric Administration numerical weather prediction and drought and flood monitoring users, the National Environmental Satellite, Data, and Information Service-Center for Satellite Applications and Research developed a global SM operational product system (SMOPS), which is a combination of all available daily SM retrievals from multiple satellite platforms (Liu et al., 2016; Yin, Zhan, Zheng, Liu, et al., 2015). The near real time SMOPS SM data including 6-hourly (00Z, 06Z, 12Z, and 18Z; 3-hr latency) and daily data (6-hr latency) files have been operationally available to users since 2013 (Liu et al., 2016).

Given the availability of the aforementioned satellite microwave SM products, it is desirable to enhance LSM skills and in turn further improvements on weather, hydrological, and climatological predictions, as well as drought and flood monitoring capabilities. Recent research has shown that data assimilation (DA) is a key approach to optimally merge the SM from model simulations and satellite observations in order to obtain the optimal estimates of the state variables and the energy and mass fluxes between land surface and the atmosphere (Crow & Wood, 2003; Evensen, 1994; Kumar et al., 2014; Rodell et al., 2004; Walker & Houser, 2001; Yin et al., 2014; Yin, Zhan, Zheng, Liu, et al., 2015). Ongoing researches show that assimilation of satellite surface SM observations has positive impacts on LSM simulations (Albergel et al., 2018; Leroux et al., 2018; Sawada, 2018). And improvements on LSM performances are implemented not only with the benefits of assimilating active SM retrievals (Brocca et al., 2017; Dharssi et al., 2011) but also with the advances of passive SM assimilation (Draper et al., 2012; Kumar et al., 2014; Li et al., 2012; Lievens et al., 2015). While the efficiency and effectiveness of assimilating microwave SM data into LSMs may be impacted by spatially and temporally continuous retrievals of SM (Kolassa et al., 2017). Thus, the assimilation of a SM product combination merging all available SM retrievals from multiple satellite sensors is expected to provide better assimilation effectiveness as long as the individual products are properly blended (Draper et al., 2012; Yin, Zhan, Zheng, Liu, et al., 2015).

What makes the SMOPS product unique is it provides a global blended SM data in near real time. Ongoing studies have indicated that model skills can be significantly enhanced with benefits of assimilating SMOPS blended (hereafter, SMOPS) SM product V2.0 that is a combination of SMOS, ASCAT, and WindSat (Nair & Indu, 2016; Yin et al., 2014, Yin, Zhan, Zheng, Liu, et al., 2015, Yin, Zhan, Zheng, Hain, et al., 2015). With the SMAP SM data becoming available, we developed the SMOPS product V3.0 that merges the SMOS, SMAP, AMSR2, ASCATA, and ASCATB SM retrievals. The SMOPS V3.0 has been operationally released since 2017, but it is still unknown the impacts of SMOPS SM V3.0 assimilation on LSM performance, and even it is unknown the metrics of assimilating the blended SM in comparison with assimilation of individual SM observations. In this paper, the following section will contain descriptions of the data sets used in this paper. Designs of DA strategy will be introduced in section 3. The results focused on differences between the SMOPS and the individual SM products, as well as intercomparison of assimilating them into the Noah LSM will be shown in section 4. The discussions relevant to interpret the detection results are provided in section 5. And finally, brief conclusions are given in section 6.

2. Data Sets

2.1. Individual SM Retrievals

Daily SMOS, ASCATA, ASCATB, AMSR2, and SMAP during 1 April 2015 to 30 June 2017 period are used in this paper. All individual SM retrievals we got from the producers were level 2 data in swath or orbit. These

data were gridded to 0.25° lat/lon grids using a simple average of all the footprint retrievals when footprint center locations fall into one grid. Before bias correlation, all of the five individual SM retrievals were quality controlled using the snow and frozen ground flags.

2.1.1. SMOS

The ESA's SMOS mission launched on 2 November 2009 was the first ever satellite mission designated for SM observation (Kerr et al., 2010). It carries the Microwave Imaging Radiometer using Aperture Synthesis. The L-band SMOS radiometer (1.400–1.427 GHz) may penetrate vegetation cover with vegetation water content up to 5 kg/m^2 and soil depth to about 5 cm (Kerr et al., 2010). From an altitude of around 758 km, the antenna views an area of almost 3,000 km in diameter at about 40-km footprint resolution (Table 1). The real-time SMOS data V6.20 is available from ESA within 3 hr from sensing time.

2.1.2. ASCAT

The ASCAT sensor is an advanced version of the scatterometer operating in C-band (5.255 GHz) on board of MetOp-A (ASCATA) and MetOp-B (ASCATB) satellites, which were launched in October 2006 and September 2012, respectively (Brocca et al., 2017). ASCAT has three radar antenna beams illuminating a continuous ground swath at three different azimuth angles (45°, 90°, and 135° sideward from the direction of the satellite motion) on both sides of the track (Brocca et al., 2017; Wagner et al., 2013). The MetOp satellites cross the equator at a Local Solar Time about 9:30 and 21:30 in descending and ascending orbit directions, respectively (Table 1). The latest version ASCATA and ASCATB data from the European Organization for the Exploitation of Meteorological Satellites are used in this paper.

2.1.3. AMSR2

The AMSR2 onboard the GCOM-W1 satellite is a remote sensing instrument for measuring weak microwave emission from the surface and the atmosphere of the Earth (JAXA, 2013). It was launched in May 2012 with the main mission of monitoring the water cycle (Maeda et al., 2016). From about 700 km above the Earth, the antenna of AMSR2 rotates once per 1.5 s and obtains data over about 1,450-km swath (Maeda et al., 2016). Equator crossing time of the GCOM-W1 satellite is about 1:30 am (1:30 pm) in descending (ascending) orbit direction (Table 1). Compared to the AMSRE, AMSR2 has several enhancements including larger main reflector and an improved calibration system and spatial resolution. The C-band (6.9 GHz) of AMSR2 is used to estimate SM. In this paper, the AMSR2 V1.0 retrieved from National Oceanic and Atmospheric Administration National Environmental Satellite, Data, and Information Service are employed.

2.1.4. SMAP

The SMAP satellite was successfully launched in January 2015 and began to provide science data in April 2015. The observatory was originally developed to provide global mapping of high-resolution SM and freeze-thaw state every 2–3 days using both L-band radar (active) and radiometer (passive). The SMAP is designed to provide SM estimations for the top 5-cm soil layer with an error less than 0.04 m^3/m^3 and penetrate vegetation cover with vegetation water content greater than 5 kg/m^2. A combination of L-band radar (active) and L-band radiometer (passive) sensors on the SMAP satellite scans a wide about 1,000-km swath from an altitude of around 685 km (Entekhabi et al., 2010). However, the SMAP radar encountered an irrecoverable hardware failure on 7 July 2015 and was officially declared lost shortly thereafter. Despite the failure of the radar instrument, the remaining SMAP radiometer (1.41 GHz) has been operating nominally, collecting high-quality brightness temperature data that enable the production of the standard level 2 Passive Soil Moisture Product and its level 3 daily composite version (Colliander et al., 2017; Reichle et al., 2017). The SMAP V5.0 data distributed by National Snow and Ice Data Center are used in this paper.

2.2. SMOPS Blended Product

Available existing individual satellite SM products currently include ASCAT from both MetOp-A (ASCATA) and MetOp-B (ASCATB) satellites (Wagner et al., 2013), AMSR2 (JAXA, 2013), the SMOS (Kerr et al., 2010), and SMAP (Entekhabi et al., 2010). However, the individual retrievals from different multiple sensors have their own characteristics and spatial resolutions (Table 1). To generate a merged global SM data product, the available observations from those satellite platforms need to be combined into one value for each grid at the same resolution. Before combining them together, all retrievals are extracted from their original formats, regridded to SMOPS 0.25° lat/lon grids, and bias corrected to Global Land Data Assimilation System (GLDAS) 0- to 10-cm SM climatology using the cumulative distribution function (CDF)-matching method (Reichle & Koster, 2004). Next, SM retrievals from SMOS L2, ASCATA L2, ASCATB L2, AMSR2 L2, and SMAP L2 (radiometer-based V-pol single channel) acquired within the previous 6-hr and 24-hr

Table 1
Descriptions of the Individual SM Retrievals Combined into the SMOPS Blended SM Product

Sensor	Band	Footprint resolution	Active/passive	Swath width (km)	Revisit time	Equator crossing (D/A)	Altitude (km)	Start of data
SMOS	L-Band	~40 km	Passive	~915	2–3 days	6:00/18:00	~758	2009
ASCAT	C-Band	25–35 km	Active	~550	2–3 days	9:30/21:30	~800	2006
AMSR-2	C-Band	24 km × 42 km	Passive	~1,450	2–3 days	1:30/13:30	~700	2012
SMAP	L-Band	39 km × 47 km	Passive	~1,000	2–3 days	9:30/21:30	~685	2015

Note. SMAP = Soil Moisture Active Passive; ASCAT = Advanced Scatterometer; SMOS = Soil Moisture and Ocean Salinity; AMSR = Advanced Microwave Scanning Radiometer for Earth Observing System.

windows are composited for the 6-hourly and daily blended products, respectively. Finally, equal weights are applied for all available retrievals to generate the daily SMOPS. In this paper, the daily 0.25° SMOPS data sets (V 3.0) are employed during 1 April 2015 to 30 June 2017 with quality control using the snow and frozen ground flags.

2.3. SCAN In Situ Observations

The U. S. Department of Agriculture Soil Climate Analysis Network (SCAN) focusing on agricultural areas of the United States is composed of over 200 sites. Hourly SM measurements with device measuring the dielectric constant of the soil are automatically screened for the limits of the sensors (Liu et al., 2011; Schaefer et al., 2007). Detection of problematic observations was applied to quality control the data sets from each SCAN site (Liu et al., 2011). Specifically, we excluded SM measurements outside of the physically possible range (Liu et al., 2011). Based on SCAN soil temperature measurements, the SM observations under frozen conditions were also excluded (Liu et al., 2011). Finally, there are a total of 113 sites for 10-cm SM validations and 105 sites for 100-cm SM validations in the contiguous United States (CONUS) were chosen by excluding sites with fewer than 183 days of observations.

2.4. Enhanced Vegetation Index

Enhanced vegetation index (EVI) has improved sensitivity in high biomass regions with reducing atmosphere influences, and it thus was developed for the Moderate Resolution Imaging Spectroradiometers (MODIS; Jiang et al., 2008). MODIS provides 8-daily EVI at 1-km spatial resolution utilizing the Aqua and Terra 16-day intervals. In this paper, the MODIS EVI data during 1 April 2015 to 30 June 2017 were retrieved and resampled to 25-km spatial resolution. The corresponding sample size is 103, since there are 103 8-days during the study period. Because of the vegetation water requirement, SM is expected to have good correlation with a vegetation index (Bolten & Crow, 2012).

3. Study Settings

3.1. Model Configuration

The Noah LSM is a one-dimensional soil-vegetation-atmosphere transfer model that is a component of the operational Global Forecast System, North American mesoscale models, North American Land Data Assimilation System, and GLDAS (Ek et al., 2003; Rodell et al., 2004; Xia et al., 2012). Four soil layers of increasing thicknesses of 10, 30, 60, and 100 cm are used to model SM dynamics (Ek et al., 2003). In the Noah LSM, the volumetric SM content (θ) prognostic equation is given by (Chen & Dudhia, 2001; Richards, 1931)

$$\frac{\partial\theta}{\partial t}=\frac{\partial}{\partial t}\left(D\frac{\partial\theta}{\partial z}\right)+\frac{\partial K}{\partial z}+F_\theta, \tag{1}$$

where F_θ represents soil water sources and sinks. The soil water diffusivity D and the hydraulic conductivity K are

$$D=K(\theta)\left(\frac{\partial\rho}{\partial\theta}\right), \tag{2}$$

$$K(\theta)=K_s(\theta/\theta_s)^{2b+3}, \tag{3}$$

$$\rho(\theta) = \rho_s/(\theta/\theta_s)^b, \tag{4}$$

where the parameters b, ρ_s, and K_s depend on soil type, wherein b and ρ indicate curve fitting parameter and soil water tension function, respectively.

3.2. Bias Correction

The Noah version 3.2 in this study was initially forced by a high-quality GLDAS precipitation data set (Rodell et al., 2004) to generate a Noah model-based 0- to 10-cm SM climatology. The Noah model is spun up by cycling 20 times through the period from 1 January 2002 to 30 June 2017, and then the simulations were conducted over the 1 April 2015 to 30 June 2017 period with 0.5-hr time step inputs and daily outputs. To satisfy the assumption that the observations and model simulations are Gaussian distributed and not biased from each other in ensemble Kalman Filter (EnKF), all of the six satellite SM products in this paper were bias corrected to climatology of Noah model-based 0- to10-cm SM estimations. The CDF-matching method having better spatial and temporal stratification was used to conduct bias corrections with CDFs built for each land grid over the whole study period in this paper (Reichle & Koster, 2004; Yin & Zhan, 2018).

3.3. Ensemble Kalman Filter

The EnKF is a widely used approach in sequential SM assimilation (Evensen, 1994). Based on generating an ensemble of model state vectors, the EnKF alternates an ensemble forecast step and a state variable update step using a Monte Carlo approximation of a sequential Bayesian filtering process (Evensen, 1994). Using perturbations to forcing data, model parameters, and state variables, the model states (F) propagated forward for each ensemble member in the forecast step is given by

$$\boldsymbol{F}^{t+} = F^{t-} + \mathbf{K}\left(\mathbf{M}^t - \mathbf{H}F^{t-}\right), \tag{5}$$

where $\mathbf{M}$, $\mathbf{H}$, and $\mathbf{K}$ are the observation vector, the observation operator, and the Kalman gain matrix, respectively.

$$\boldsymbol{K} = \frac{\xi_F^t \mathbf{H}^{t\mathbf{T}}}{\mathbf{H}^t \xi_F^t \mathbf{H}^{t\mathbf{T}} + \xi_M^t} \tag{6}$$

The matrix $\mathbf{H}$ depends on the observations. And ξ_M^t is error variance for measurements. Forecast error variance ξ_F^t is determined by the ensemble spread. Specifically, the error variances used a constant value (3%) as Land Information System (LIS) examples using Kumar et al. (2009). Our particular application used 12-member ensemble (Yin, Zhan, Zheng, Hain, et al., 2015) to update all four Noah SM states (0–10 cm, 10–40 cm, 40–10 cm, and 100–200 cm) using either SMOPS blended or individual SM retrievals. Perturbations of both forcing data and state variables are applied at each individual 30-min Noah model time step.

3.4. DA Strategy

The basic DA structure used to intercompare the performances of assimilating SMOPS and individual SM retrievals is summarized as follows:

1. The control (CTR) run represents the Noah LSM runs with the unperturbed forcing data and state variables. It indicates Noah model simulations without benefits of satellite SM assimilation. As introduced in section 3.2, all of the satellite SM retrievals were bias corrected to the 0- to 10-cm SM simulations from the CTR run.
2. An open loop (OLP) run was set as the Noah LSM runs with the perturbed forcing data according to Table 2, which is same with LIS examples using Kumar et al. (2009). It indicates the Noah model performs without the benefits of assimilating satellite SM observations under suboptimal forcing and initialization conditions. The implicit assumption is that adding unbiased noise to the forcing and state variables in the EnKF should not cause a systematic error in model output between perturbed and unperturbed state variables conditions (Ryu et al., 2009).
3. In the DA cases, the bias-corrected SM retrievals were assimilated into the OLP run. It means all of the DA cases were forced by the perturbed meteorological forcing inputs and state variables that used in the OLP run. And thus, the differences between the DA case and the OLP run are good metrics to

Table 2
Perturbation Parameters for Meteorological Forcing Parameters and State Variables (Kumar et al., 2009; Peters-Lidard et al., 2008)

Perturbation type	SD				
		Cross correlation for forcing variable perturbations			
		Precipitation	SW	LW	
Precipitation	0.5 (mm)	1.0	−0.8	0.5	
SW	0.3 (Wm^{-2})	−0.8	1.0	−0.5	
LW	50 (Wm^{-2})	0.5	−0.5	1.0	
		Cross correlation for state variable perturbations			
		SM1	SM2	SM3	SM4
SM1 (0–10 cm)	6.00×10^{-3} m^3/m^3	1.0	0.6	0.4	0.2
SM2 (10–40 cm)	1.10×10^{-4} m^3/m^3	0.6	1.0	0.6	0.4
SM3 (40–100 cm)	6.00×10^{-5} m^3/m^3	0.4	0.6	1.0	0.6
SM4 (100–200 cm)	4.00×10^{-5} m^3/m^3	0.2	0.4	0.6	1.0

Note. SW = shortwave radiation; LW = longwave radiation; SD = standard deviation. SM1, SM2, SM3, and SM4 indicate 0- to 10-cm, 10- to 40-cm, 40- to 100-cm, and 100- to 200-cm soil moisture.

investigate the performances of assimilating satellite SM retrievals. Specifically, to intercompare Noah model skills with benefits of assimilating SMOPS SM data and individual SM retrievals, the DA_SMOPS assimilates the SMOPS SM data, while the DA_SMOS, DA_SMAP, DA_AMSR, DA_ASCATA, and DA_ASCATB assimilate the SMOS, SMAP, AMSR2, ASCATA, and ASCATB retrievals, respectively.

The CTR run is a single realization (section 3.2), while the ensemble size for the OLP run and the 6 DA cases was set as 12 that is the optimal ensemble size in a sequential SM assimilation system (Yin, Zhan, Zheng, Hain, et al., 2015). The Noah model under the ensemble condition was spun up by cycling 30 times through the period from 1 April 2015 to 30 June 2017, and then all of the six DA cases and the OLP run were conducted over the same period with 30-min time step inputs and daily outputs. The daily satellite SM data in this paper were assimilated into Noah model at each 00Z run with providing updated 0- to 10-cm SM condition. The forcing data used in this paper include precipitation from the GLDAS and downward shortwave radiation, downward longwave radiation, near-surface air temperature, near-surface humidity, near-surface wind, and surface pressure from the Global Data Assimilation System product (Rodell et al., 2004).

All simulations in this paper were conducted over a gridded near-global domain (from −60°S, −180°W to 90°N, 180°E) at 25-km spatial resolution with 30-min time step inputs and daily outputs. Implementing the same variable inputs and meteorological forcing data, Noah model was run for each of the six DA cases. Differences among the DA cases are based only on assimilating different satellite SM retrievals and can thus be used to intercompare model skills with benefits of assimilating different SM retrievals.

3.5. Performance Measurements

The root mean square error (RMSE) is widely used to evaluate the differences between model simulations and ground observations. Here the RMSE is employed to assess differences of LIS-Noah 3.2 model simulations (CTR run, OLP run, and all six DA cases) and SCAN in situ measurements, which is given by

$$\boldsymbol{RMSE} = \sqrt{\frac{\sum_{i=1}^{i=N}(S_i - M_i)^2}{\sum_{i=1}^{i=N} i}}, \tag{7}$$

where S and M are model and measured variables, respectively; N is the total day number within the study period. Similarly, root mean square deviation (RMSD) is used to estimate the differences between DA_SMOPS and each of the five individual DA cases as

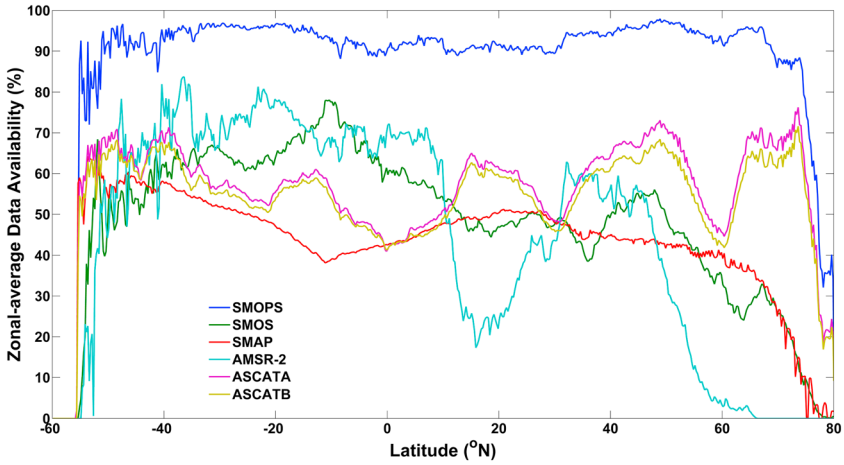

Figure 1. Zonal-average data availability (%) for SMOPS and each of the five individual satellite remote sensing SM observations. SM = soil moisture; SMOPS = Soil Moisture Operational System-Blended product; SMAP = Soil Moisture Active Passive; ASCAT = Advanced Scatterometer; SMOS = Soil Moisture and Ocean Salinity.

$$\boldsymbol{RMSD} = \sqrt{\frac{\sum_{i=1}^{i=N}\left(S(DA\_SMOPS)_i - S(DA\_Individual)_i\right)^2}{\sum_{i=1}^{i=N} i}}, \tag{8}$$

where S (DA_SMOPS) and S (DA_individual) are simulations of DA_SMOPS and individual DA cases, respectively.

4. Results

4.1. Spatial Coverage

This study is based on assimilating daily individual and blended SM retrievals during 1 April 2015 to 30 June 2017 period. Individual SM retrievals may have temporal gaps that may be filled in the blended SM product. We thus first evaluate "Data Availability" defined as the fraction of available day number over total day number during the study period for each land grid. Figure 1 shows zonal-averaged data availability (ZDA, %) for SMOPS and each of the five individual satellite remote sensing SM observations. The ZDA for SMAP presents the lowest values (40–60%) from −60°N to 50°N except in the 10–30°N area where the ZDA for the AMSR2 is below 20%. A salient feature for both ASCATA and ASCATB products is that they have higher ZDAs in the Northern Hemisphere in comparison with the passive SM retrievals, and more so in the high latitude areas. The SMOS and AMSR2

present larger ZDAs with the SMOS general higher than the AMSR2 in the −60–10°N areas. Over the entire global domain, the SMOPS has the highest ZDA (≥90%) steadily.

Relative to the AMSR2, the ZDA can be significantly enhanced by larger than 70% in the Sahara, Russia, the central Asia, and the northern Canada areas by the SMOPS (Figure 2). The status for the SMOS over the aforementioned regions is slightly improved, still 40–70% ZDA reduction can be found in comparison with the SMOPS. Besides, remarkable improvements on the SMAP ZDA by SMOPS are shown on the entire global domain, with the larger values mainly exhibiting in the Eurasia, North America, and the tropical rain forests. Compared to the ASCAT SM products, SMOPS may increase larger than ZDA in four belt areas located in −25°N, equatorial, 30°N and 60°N, respectively.

4.2. Intercomparison of the Bias-Corrected SM Retrievals

To satisfy the assumption that uncertainties of model simulations and satellite observations are all unbiased distributed, all SM retrievals were bias corrected to the Noah model-based SM climatology for the 0- to 10-cm soil layer using the CDF-matching method (section 3.2). The dryness and the wetness patterns of the daily averaged SMOPS product are reasonable as expected (Figure 3a). The larger SM values can be found in the tropical rain forest areas, northern Eurasia, eastern United States, and the southeastern China. And

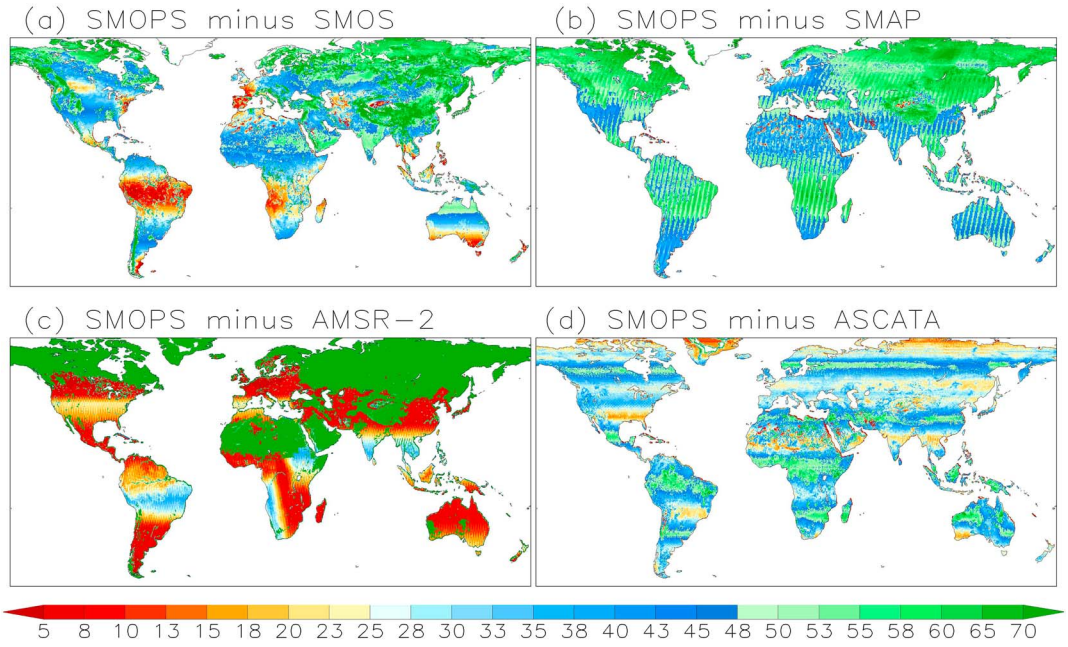

Figure 2. Improved data availability (%) by SMOPS over (a) SMOS, (b) SMAP, (c) AMSR2, and (d) ASCATA. Patterns for ASCATA and ASCATB are very similar. SMOPS = Soil Moisture Operational Product System; SMAP = Soil Moisture Active Passive; ASCAT = Advanced Scatterometer; SMOS = Soil Moisture and Ocean Salinity; AMSR = Advanced Microwave Scanning Radiometer for Earth Observing System.

the drier regions locate in the Sahara Desert, Australia, west United States, central Eurasia, and the Arabian Peninsula (Figure 3a).

The goal of this study is to intercompare the impacts of assimilating SMOPS and individual SM retrievals on the Noah model performance. We first examined the differences in the bias-corrected SM between the SMOPS and each individual SM products. Shading in red (blue) color in Figures 3b–3d indicates the SMOPS has dryer (wetter) climatology than the individual SM retrievals. Relative to SMOS, SMOPS shows drier patterns on the entire global domain (Figure 3b). Similarly, SMOPS also shows drier climatology in comparison with SMAP except in the South Africa, northwest Australia, and east Russia. Relative to SMAP, SMOPS shows the highest reduction ($\geq$0.05 m^3/m^3) of SM climatology in the tropical rain forest areas (Figure 3c). Compared to AMSR2, however, SMOPS (Figure 3d) exhibits lower daily-averaged SM in the Africa, India, the Indo-China Peninsula, and the Central and South America. Over the SMOPS product, the bias-corrected SM retrievals from the active sensors tend to express a dryer pattern in the large daily-averaged SM areas and a wetter pattern in the dry areas (Figure 3e). Situations for the ASCATA and ASCATB are very similar, and thus, the ASCATB is not shown in this paper.

Dynamics of the bias-corrected satellite observations are measured using the standard deviation (SD) in this paper (Figure 4). The SMOPS presents larger dynamics in the sub-Sahara, the Middle East, India, the southern Tibet Plateau, the west United States, and north Australia (Figure 4a). Lower SD values for the SMOPS can be seen not only in the densely vegetated areas including the tropical rain forest areas, east United States, west Europe, and south China but also in the dry areas including the Sahara Desert and the southwest China.

Differences in dynamics between SMOPS and the individual SM observations can be found in Figures 4b–4d. Shadings in red (blue) color indicate SMOPS has smaller (larger) dynamic than the individual SM retrievals. In general, AMSR2 shows a good agreement in dynamics with the SMOPS (Figure 4d), and their SD differences range from −0.01 m^3/m^3 to 0.01 m^3/m^3. Over SMOS, however, SMOPS exhibits smaller SD values in the Sahara Desert, Eurasia, and the Central America (Figure 4b). SMOPS also presents a more stable dynamic in comparison with SMAP on the entire global domain (Figure 4c). The largest reduction produced by the SMOPS can reach to lower than −0.05 m^3/m^3 in the Amazon and the Central Africa (Figure 4c). SMOPS expresses clear extension ($\geq$0.05 m^3/m^3) in dynamics over the ASCAT products in western China, Scandinavia countries, northwest United States, and western Canada in comparison with

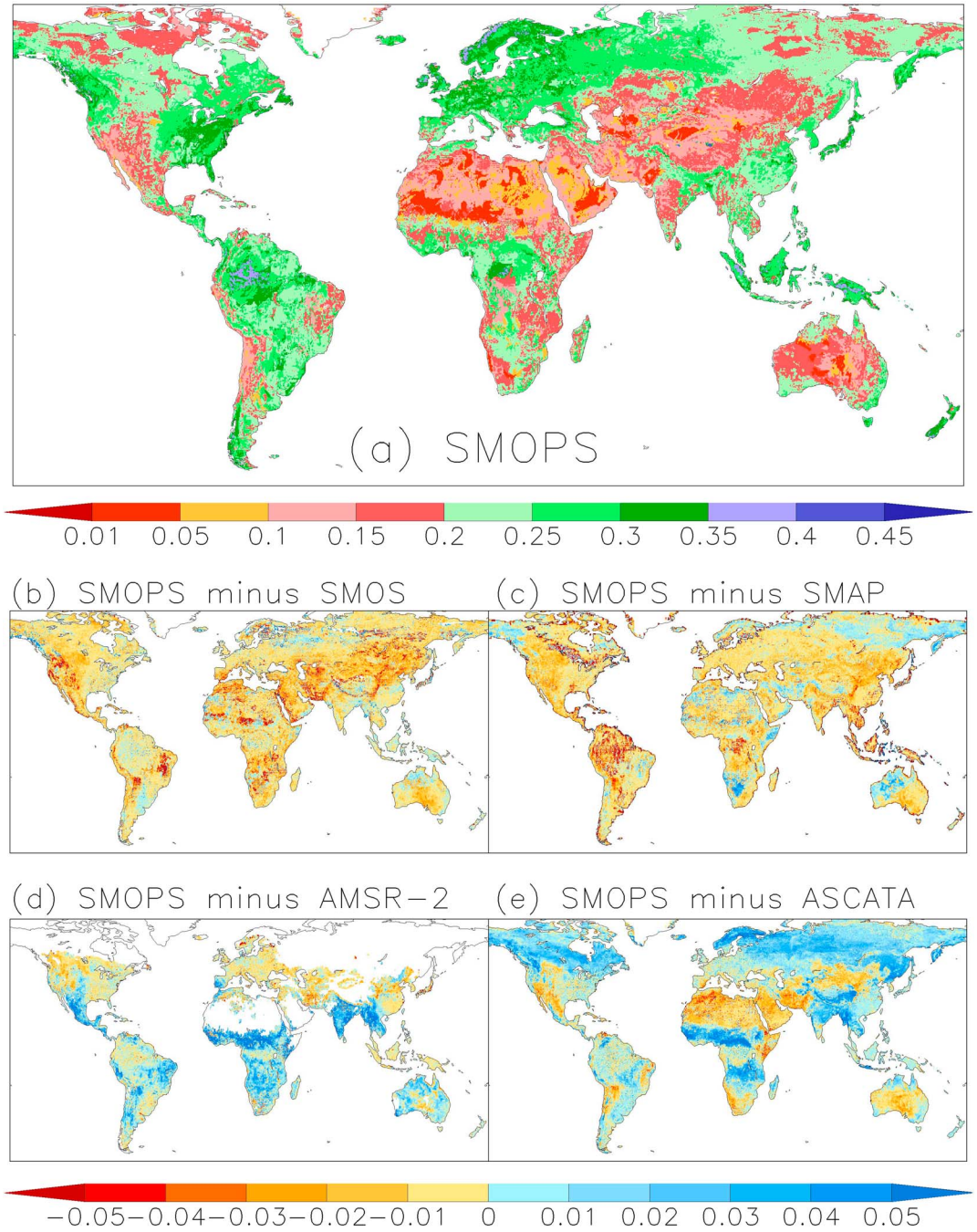

Figure 3. All SM retrievals were bias corrected to the climatology of Noah model SM simulations for the 0- to 10-cm soil layer using the CDF-matching method: (a) average SM for the bias-corrected SMOPS (m^3/m^3), followed by the differences in bias-corrected SM average (m^3/m^3) between the SMOPS and (b) SMOS, (c) SMAP, (d) AMSR2 and (e) ASCATA from 1 April 2015 to 30 June 2017. Patterns for ASCATA and ASCATB are very similar. CDF = cumulative distribution function; SM = soil moisture; SMOPS = Soil Moisture Operational Product System; SMAP = Soil Moisture Active Passive; ASCAT = Advanced Scatterometer; SMOS = Soil Moisture and Ocean Salinity; AMSR = Advanced Microwave Scanning Radiometer for Earth Observing System.

the ASCATA. Yet SMOPS exhibits lower SD values in the Sahara, Arabian Peninsula, and northwestern China (Figure 4e).

4.3. Impacts of Assimilating Different SM Retrievals on Model Outputs

Figure 5 shows spatial distributions of RMSD for 10-cm SM (m^3/m^3) between DA_SMOPS and each individual SM DA cases during 1 April 2015 to 30 June 2017 period. The larger differences (≥0.08 m^3/m^3)

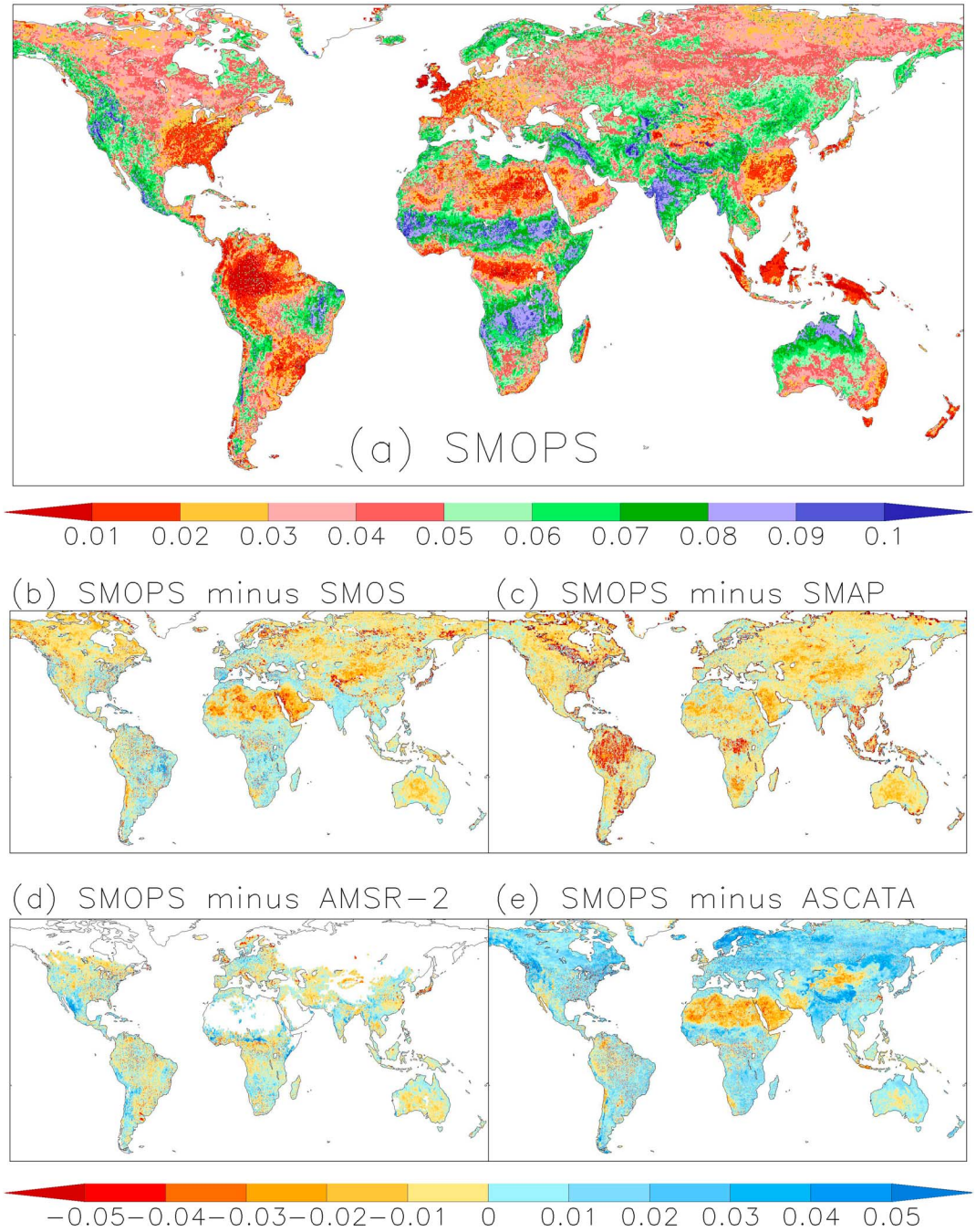

Figure 4. All SM retrievals were bias corrected to the climatology of Noah model SM simulations for the 0- to 10-cm soil layer using the CDF-matching method. (a) SD for the SMOPS (m^3/m^3), followed by the differences in SD (m^3/m^3) between SMOPS and (b) SMOS, (c) SMAP, (d) AMSR2 and (e) ASCATA over 1 April 2015 to 30 June 2017 period. Patterns for ASCATA and ASCATB are very similar. CDF = cumulative distribution function; SM = soil moisture; SMOPS = Soil Moisture Operational Product System; SMAP = Soil Moisture Active Passive; ASCAT = Advanced Scatterometer; SMOS = Soil Moisture and Ocean Salinity; AMSR = Advanced Microwave Scanning Radiometer for Earth Observing System; SD = standard deviation.

in the 10-cm SM between DA_SMOPS and the three DA cases using the passive SM retrievals can be found in northern Eurasia and northern North America (Figure 5), corresponding larger data availability differences (Figure 2). Outside of the dry areas, lower RMSD values ($\leq$0.03 m^3/m^3) between DA_SMOPS and each of the three passive SM DA cases (DA_SMOS, DA_SMAP, and DA_AMSR) can be seen in the tropical rain forests, eastern United States, southeast China, and the eastern Australia. RMSD between DA_SMOPS and

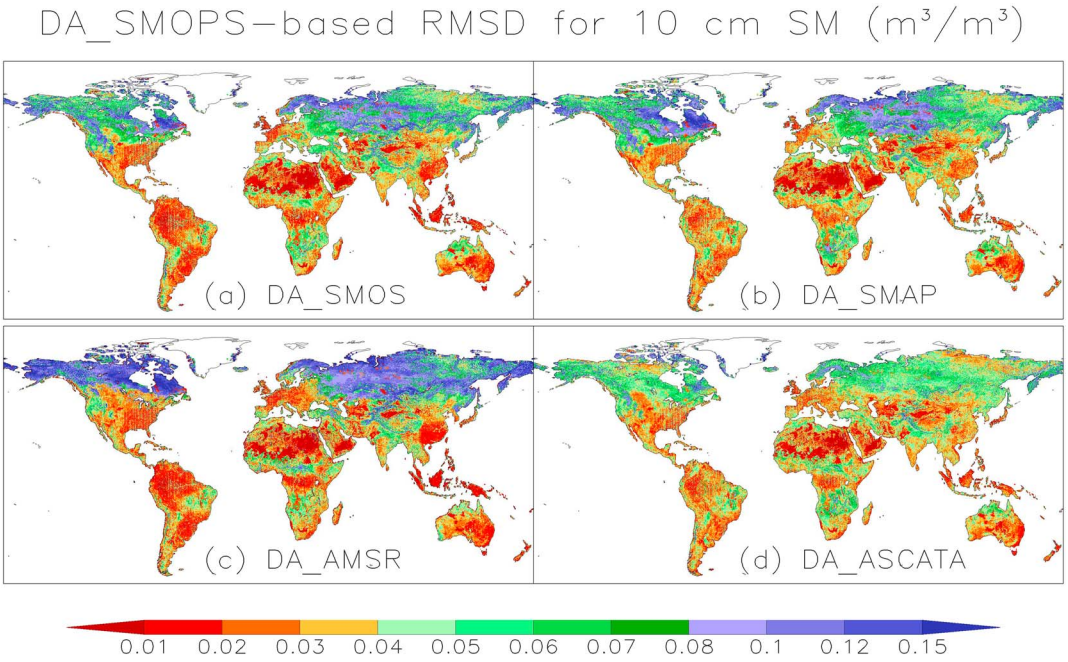

Figure 5. Spatial distributions of RMSD for 10-cm SM (m^3/m^3) between DA_SMOPS and (a) DA_SMOS, (b) DA_SMAP, (c) DA_AMSR and (d) DA_ASCATA during 1 April 2015 to 30 June 2017 period. Patterns for DA_ASCATA and DA_ASCATB are very similar. DA = data assimilation; SM = soil moisture; SMOPS = Soil Moisture Operational Product System; SMAP = Soil Moisture Active Passive; ASCAT = Advanced Scatterometer; SMOS = Soil Moisture and Ocean Salinity; AMSR = Advanced Microwave Scanning Radiometer for Earth Observing System; SD = standard deviation; RMSD = root mean square deviation.

DA_ASCATA presents a similar spatial pattern with the larger value distributed in northern Eurasia and northern North America, while the magnitude is clearly reduced (Figure 5d).

4.4. Model Performance Evaluation Using SCAN In Situ Observations

Figure 6 shows spatial RMSE distributions of DA_SMOPS-based SM for surface soil layer with respect to the quality controlled SCAN observations. In general, the Noah model with benefits of assimilating SMOPS product performs reasonably in the Great Plains and the northern United States, where the RMSE values are lower than 0.1 m^3/m^3. However, the higher uncertainties can be primarily found in the western maintain areas and southeast densely vegetated areas.

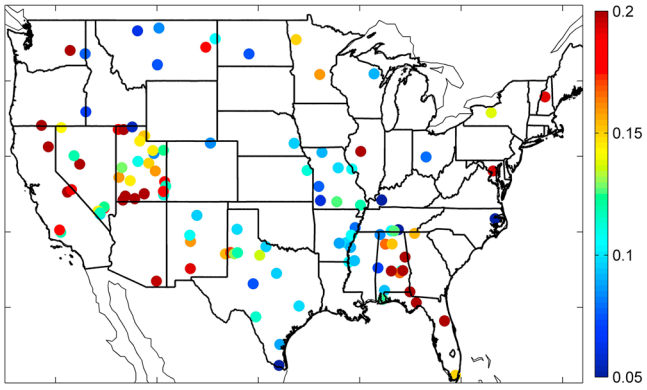

Figure 6. With respect to SCAN observations, RMSE for DA_SMOPS-based 0- to 10-cm SM simulations during 1 April 2015 to 30 June 2017 period. SM = soil moisture; DA = data assimilation; SMOPS = Soil Moisture Operational Product System; RMSE = root mean square error; SCAN = Soil Climate Analysis Network.

With the same meteorological forcing data and state variables, Figures 7a–7d show differences in SCAN observations-based RMSEs for 0- to 10-cm soil layer between the DA_SMOPS case and individual DA cases. Compared to assimilation of L-band passive SM retrievals (Figures 7a and 7b), DA_SMOPS is successful to estimate the 0- to 10-cm SM with significantly reducing the RMSE values on the CONUS domain with larger improvements exhibiting in the western and northeast United States. Compared to the L-band DA cases, while slight degradations caused by assimilating the SMOPS SM data are primarily found in central-south CONUS. With benefits of DA_SMOPS, the CONUS domain-averaged RMSEs are decreased by 0.012 m^3/m^3 (8.86% reduction) and 0.015 m^3/m^3 (11.39% reduction) in comparison with DA_SMOS and DA_SMAP cases, respectively (Table 3c). Differences in model capability of 0- to 10-cm SM estimations between DA_SMOPS and DA_ASCATA cases exhibit similar spatial patterns with DA_SMOPS showing obvious improvements in the western and northeast United States (Figure 7d). Because of the duplicate distributions, spatial patterns for the DA_ASCATB case are not denoted here. Relative to

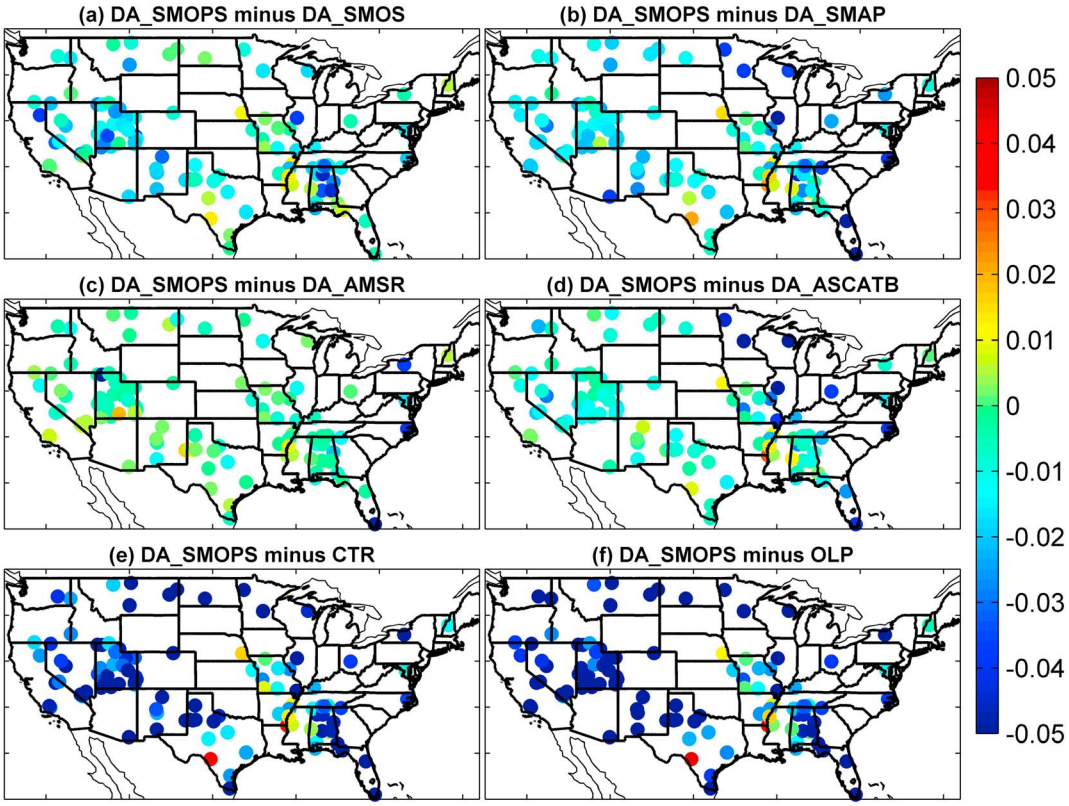

Figure 7. Differences in SCAN observations-based RMSE for 0- to 10-cm soil layer during 1 April 2015 to 30 June 2017 period: (a) DA_SMOPS minus DA_SMOS, (b) DA_SMOPS minus DA_SMAP, (c) DA_SMOPS minus DA_AMSR, (d) DA_SMOPS minus DA_ASCATA, (e) DA_SMOPS minus CTR, and (f) DA_SMOPS minus OLP. Patterns for DA_ASCATA and DA_ASCATB are very similar. DA = data assimilation; SCAN = Soil Climate Analysis Network; RMSE = root mean square error; CTR = control run; OLP = open loop run; SMOPS = Soil Moisture Operational Product System; SMAP = Soil Moisture Active Passive; ASCAT = Advanced Scatterometer; SMOS = Soil Moisture and Ocean Salinity; AMSR = Advanced Microwave Scanning Radiometer for Earth Observing System; SD = standard deviation.

DA_ASCATA and DA_ASCATB cases, the CONUS domain-averaged uncertainties of SM simulations for the surface soil layer are reduced by 0.010 m^3/m^3 (6.73% reduction) and 0.011 m^3/m^3 (8.33% reduction) by the DA_SMOPS (Table 3c). Relatively, the DA_SMOPS presents a slight improvement on 0- to 10-cm SM simulation with a 3.09% noise decrement in comparison with the DA_AMSR (Figure 7c; Table 3c).

With respect to the SCAN measurements, DA_SMOPS shows a significant improvement on Noah model 0- to 10-cm SM simulations over both of the CTR and OLP runs in the eastern, western, and northern CONUS, where the model uncertainties can be reduced larger than 0.05 m^3/m^3 with benefits of assimilating SMOPS SM observations (Figures 7e and 7f). Yet weak degradations caused by assimilation of SMOPS SM data can be found in central-south CONUS where DA_SMAP, DA_SMOS, and DA_ASCATA have better performance over the DA_SMOPS case. The statistical results demonstrate that the CONUS domain-averaged RMSEs are decreased by 0.040 m^3/m^3 (27.14% reduction) and 0.047 m^3/m^3 (32.11% reduction) with benefits of SMOPS SM assimilation in comparison with the CTR and OLP runs, respectively (Table 3c).

Additionally, relative to RMSE reductions over individual DA cases, improvements of assimilating SMOPS SM data on model surface SM estimations are more remarkable in comparison with the OLP and CTR cases. It indicates that all of the individual DA cases exhibit clear enhancements on Noah model skill of estimating SM for the surface soil layer. Specifically, compared to the OLP run, the CONUS domain-averaged RMSE values can be decreased by 0.035 m^3/m^3 (23.90%), 0.032 m^3/m^3 (21.09%), 0.043 m^3/m^3 (30.59%), 0.036 m^3/m^3 (25.19%), and 0.034 m^3/m^3 (23.15%) by the DA_SMOS, DA_SMAP, DA_AMSR, DA_ASCATA, and DA_ASCATB, respectively (Table 3a). Similarly, relative to the CTR run, the domain-averaged RMSE values are reduced by 0.028 m^3/m^3 (19.17%), 0.025 m^3/m^3 (16.46%), 0.036 m^3/m^3 (25.16%), 0.029 m^3/m^3 (20.41%), and 0.027 m^3/m^3 (18.43%) by the DA_SMOS, DA_SMAP, DA_AMSR, DA_ASCATA, and DA_ASCATB,

Table 3
With Respect to SCAN In Situ Observations, Statistics for CONUS Domain-Averaged RMSE Differences and the Corresponding Difference Percentages During 1 April 2015 to 30 June 2017 Period

DA Cases	10 cm SM (m^3/m^3)	100 cm SM (m^3/m^3)	10 cm SM (%)	100 cm SM (%)
(a)				
	RMSE Diff_a		P_{Diff_a}	
DA_SMOS	0.035	0.034	23.90	24.06
DA_SMAP	0.032	0.034	21.09	24.07
DA_AMSR	0.043	0.033	30.59	23.59
DA_ASCATA	0.036	0.040	25.19	30.01
DA_ASCATB	0.034	0.035	23.15	24.99
DS_SMOPS	0.047	0.029	34.89	18.89
(b)				
	RMSE Diff_b		P_{Diff_b}	
DA_SMOS	0.028	0.033	19.17	23.24
DA_SMAP	0.025	0.033	16.46	23.26
DA_AMSR	0.036	0.032	25.61	22.77
DA_ASCATA	0.029	0.040	20.41	29.15
DA_ASCATB	0.027	0.035	18.43	24.17
DS_SMOPS	0.040	0.028	29.72	18.13
(c)				
	RMSE Diff_c		P_{Diff_c}	
DA_SMOS	0.012	−0.005	8.86	−3.31
DA_SMAP	0.015	−0.005	11.39	−3.31
DA_AMSR	0.004	−0.004	3.28	−2.96
DA_ASCATA	0.011	−0.012	7.74	−7.53
DA_ASCATB	0.013	−0.006	9.53	−4.00

Note. DA = data assimilation; OLP = open loop run; CTR = control run; RMSE = root mean square error; CONUS = contiguous United States; SCAN = Soil Climate Analysis Network; SM = soil moisture; SMOPS = Soil Moisture Operational Product System; SMAP = Soil Moisture Active Passive; ASCAT = Advanced Scatterometer; SMOS = Soil Moisture and Ocean Salinity. (a) Between DA case and OLP run, and the *Diff_a* and the P_{Diff_a} are given by $Diff\_a = \mathrm{RMSE}(DA) - \mathrm{RMSE}(\mathrm{OLP})$, and $P_{Diff\_a} = \frac{Diff\_a}{\mathrm{RMSE(DA)}} \times 100\%$; (b) between DA case and CTR run, and the *Diff_b* and the P_{Diff_b} are given by $Diff\_b = \mathrm{RMSE}(DA) - \mathrm{RMSE}(\mathrm{CTR})$, and $P_{Diff\_b} = \frac{Diff\_b}{\mathrm{RMSE(DA)}} \times 100\%$; (c) between DA_SMOPS and each of the five individual DA cases (x), and the *Diff_c* and the P_{Diff_c} are given by $Diff\_c = \mathrm{RMSE}(x) - \mathrm{RMSE}(\mathrm{DA\_SMOPS})$, and $P_{Diff\_c} = \frac{Diff\_c}{\mathrm{RMSE(DA\_SMOPS)}} \times 100\%$. The positive (negative) values in (a) and (b) indicate improvement (degradation) caused by satellite SM assimilation over OLP and CTR runs, respectively. While positive (negative) value in (c) means DA_SMOPS performs better (worse) in comparison with individual DA cases.

respectively (Table 3b). Implication of the results denotes improvements on model 0–10 SM simulations are evident with benefits of assimilating not only the blended SM data but also individual SM retrievals.

However, the positive signals from the surface soil layer are not completely vertically propagated to the deeper soil layer. With respect to the SCAN observations, DA_SMOPS shows lower RMSEs in west and southeast CONUS in comparison with each of the five individual DA cases (Figures 8a–8d). It can be also found that RSMEs for both CTR and OLP runs are significantly reduced with benefits of assimilating SMOPS blended SM data (Figures 8e and 8f). Yet DA_SMOPS presents clearly negative impacts on model performance in Mississippi river region and Texas (Figure 8) where DA_SMOPS shows slight improvements on 0- to 10-cm Noah LSM-based SM estimations (Figure 7).

Statistics document that DA_SMOPS presents significant improvements on root zone SM simulations in comparison with the CTR and OLP runs, but the ~30% benefits for the 0- to 10-cm soil layer are reduced to about 18% for the root zone soil layer (Tables 3a and 3b). Besides, compared to the DA_SMOS, DA_SMAP, DA_AMSR, DA_ASCATA, and DA_ASCATB cases, the CONUS domain-averaged RMSEs are slightly increased by 0.005 m^3/m^3 (3.31% increase), 0.005 m^3/m^3 (3.31% increase), 0.004 m^3/m^3 (2.96% increase), 0.012 m^3/m^3 (7.53% increase), and 0.006 m^3/m^3 (4.00% increase), respectively (Table 3c). Relatively, it can also be found the significant improvements of assimilating individual SM retrievals on the root zone SM estimations in comparison with the CTR and OLP runs. Particularly, relative to the OLP run, the CONUS domain-averaged RMSE values can be reduced by 0.034 m^3/m^3 (24.06%), 0.034 m^3/m^3

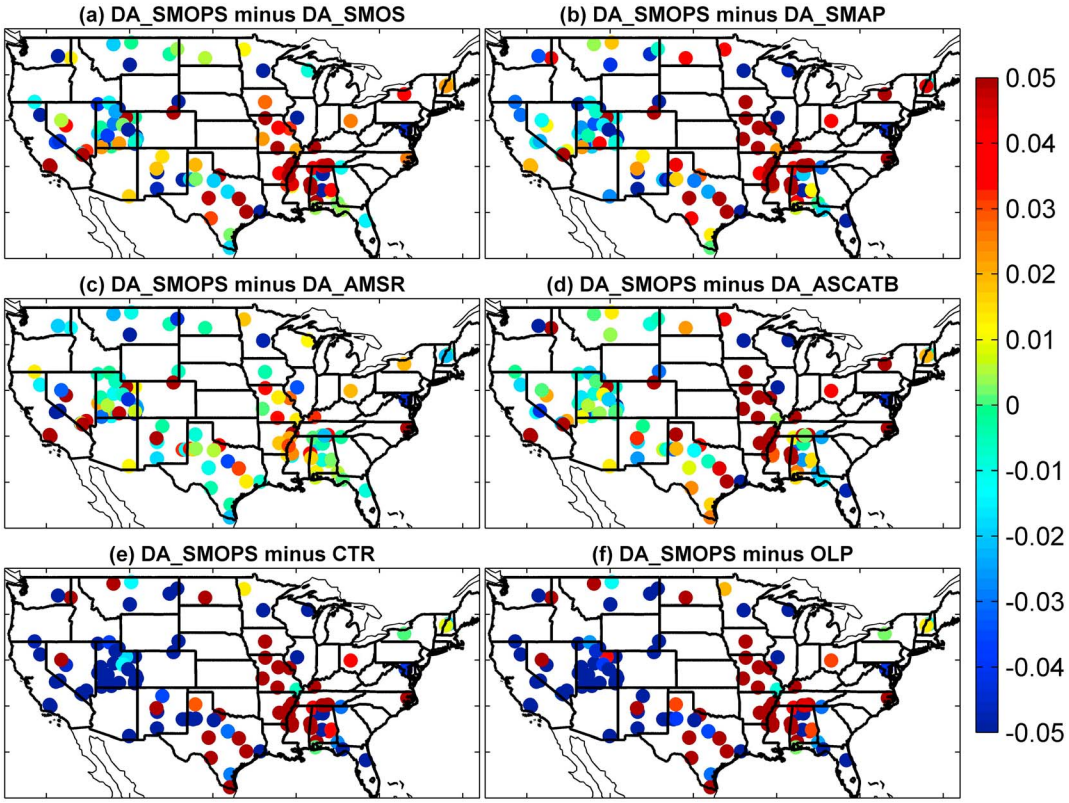

Figure 8. Differences in SCAN observations-based RMSE for 0- to 100-cm soil layer during 1 April 2015 to 30 June 2017 period: (a) DA_SMOPS minus DA_SMOS, (b) DA_SMOPS minus DA_SMAP, (c) DA_SMOPS minus DA_AMSR, (d) DA_SMOPS minus DA_ASCATA, (e) DA_SMOPS minus CTR, and (f) DA_SMOPS minus OLP. Patterns for DA_ASCATA and DA_ASCATB are very similar. DA = data assimilation; SCAN = Soil Climate Analysis Network; RMSE = root mean square error; CTR = control run; OLP = open loop run; SMOPS = Soil Moisture Operational Product System; SMAP = Soil Moisture Active Passive; ASCAT = Advanced Scatterometer; SMOS = Soil Moisture and Ocean Salinity; AMSR = Advanced Microwave Scanning Radiometer for Earth Observing System; SD = standard deviation.

(24.07%), 0.033 m^3/m^3 (23.59%), 0.040 m^3/m^3 (30.01%), and 0.035 m^3/m^3 (24.99%) by the DA_SMOS, DA_SMAP, DA_AMSR, DA_ASCATA, and DA_ASCATB, respectively (Table 3a). Compared to the CTR run, the domain-averaged RMSE values are decreased by 0.033 m^3/m^3 (23.24%), 0.033 m^3/m^3 (23.26%), 0.032 m^3/m^3 (22.77%), 0.040 m^3/m^3 (29.15%), and 0.035m^3/m^3 (24.17%) by the DA_SMOS, DA_SMAP, DA_AMSR, DA_ASCATA, and DA_ASCATB, respectively (Table 3b).

4.5. Complementary Evaluations on Model Performance

With respect to the quality controlled SCAN observations, validations in section 4.4 clearly show the good metrics from all of the DA cases over the OLP and CTR runs, and the DA_SMOPS presents the best performance in surface soil layer. However, in situ SM measurements are generated from low density networks and limited in spatial representativeness on entire global domain (Koster et al., 2009; Yin, Zheng, et al., 2015). Due to SM is a regulator of plant growth through impacting photosynthesis and biomass allocation, there are positive relationships between SM and vegetation status that can be well expressed using the vegetation indices. Comparison with the gridded vegetation index products is thus an important complementary evaluation on the model SM simulations (Dorigo et al., 2017). To match the temporal resolution of the MODIS-EVI product, model SM estimations were temporally resampled from daily to 8-daily in this paper. The surface SM simulations from the DA_SMOPS show robust agreements with the MODIS_EVI for a lag of SM preceding EVI by 8 days in Central America, northern North America, eastern South America, Sub-Saharan Africa, the western Australia, and central-eastern Eurasia (Figure 9). In the other areas such as western Eurasia, western United States, and eastern United States (Dorigo et al., 2017), however, the SM for top surface soil layer shows negative correlations with the MODIS EVI.

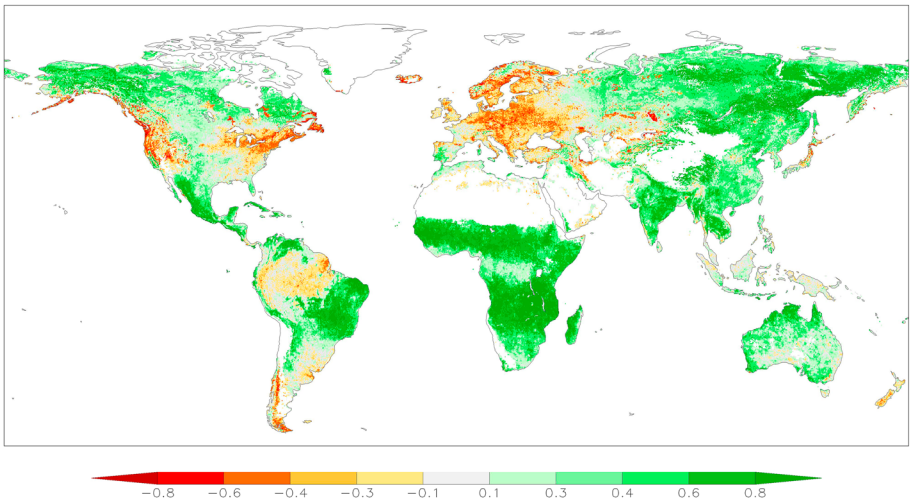

Figure 9. Pearson correlations between 8-daily DA_SMOPS-based 0- to 10-cm SM and MODIS EVI over 1 April 2015 to 30 June 2017 study period for a lag of SM preceding EVI by 8 days. DA = data assimilation; SMOPS = Soil Moisture Operational Product System; SM = soil moisture.

With respect to 8-daily MODIS EVI, Figures 10a–10d show differences in Pearson correlations for 0- to10-cm SM simulations between DA_SMOPS and individual DA cases over 1 April 2015 to 30 June 2017 study period for a lag of SM preceding EVI by 8 days. Shading in blue (red) color means DA_SMOPS has stronger (weaker) correlations with the MODIS-EVI data. The DA_SMOPS-based SM estimations for the topsoil layer show slight enhancements on the correlations with the MODIS EVI in the southern South America, south Africa, and the central Australia over the three passive DA cases including DA_SMOS (Figure 10a), DA_SMAP (Figure 10b), and DA_AMSR (Figure 10c). With regards to central and northern Eurasia and northern North America, DA_SMOPS presents more robust agreement with the MODI_EVI product (Figures 10a–10c) with enhancing the correlation coefficients higher than 0.5 (Figures 10a–10c). However, the differences in Pearson correlations between the DA_SMOPS and the DA_ASCATA cases are clearly reduced with DA_SMOPS showing slight improvements in east Eurasia and west North America (Figure 10d), whereas slight degradations are found in the west Russia and east North America (Figure 10d).

Relative to the CTR run, Noah model SM simulations for 0- to 10-cm soil layer with benefits of assimilating the SMOPS SM product exhibit more robust correlations with the MODIS-EVI data in Eurasia, Canada, and west United States (Figure 10e). Yet degradations caused by the DA_SMOPS are found in east CONUS, the Arabian Peninsula, central Australia, South Africa, and the southern South America. Additionally, the DA_SMOPS presents much stronger agreement with the 8-daily MODIS EVI in comparison with the OLP run (Figure 10f) with the improvements dominating the global domain except slight degradations primarily distributed in South America and east CONUS.

With respect to 8-daily MODIS EVI, the zonal-averaged Pearson correlation differences between DA_SMOPS and each individual DA case, CTR and OLP runs for lags of SM preceding EVI by 8 days (red), 16 days (blue), 24 days (green), and 32 days (black) are shown in Figure 11. Good agreements can be seen for lags of SM preceding EVI by 8, 16, 24, and 32 days with ranked correlation for EVI lagged 8 days generally showing higher temporal correlations (Figure 11). Over each passive DA case, Pearson correlations between DA_SMOPS-based 0- to 10-cm SM simulations and MODIS EVI data sets present clear improvements in areas north of 35°N (Figures 11a–11c). Whereas statistical results relative to the individual DA cases do not show the remarkable differences in the root zone for lags of SM preceding EVI by 8, 16, 24, and 32 days. Relative to DA_ASCATA case, the DA_SMOPS presents a little better agreement with the 8-day MODIS EVI in the north areas of 45°N (Figure 11d).

The CTR and OLP runs demonstrate similar patterns with showing the most modest performance in 50–60°N areas (Figures 11e and 11f) in comparison with DA_SMOPS case. With benefits of assimilating SMOPS SM data, enhancements on MODIS-EVI-based correlations can reach to 0.8 in the north areas of

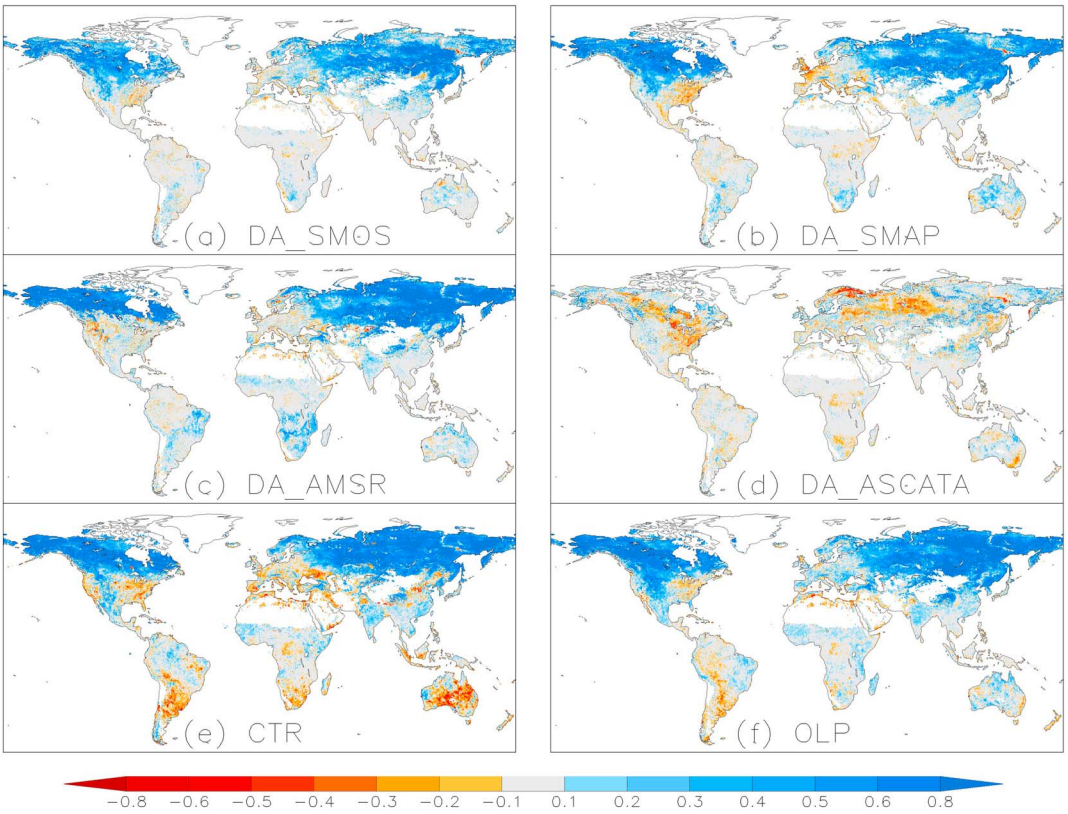

Figure 10. With respect to 8-daily MODIS EVI, differences in Pearson correlations for 0- to 10-cm SM simulations between DA_SMOPS and (a) DA_SMOS, (b) DA_SMAP, (c) DA_AMSR, (d) DA_ASCATA, (e) CTR, and (f) OLP cases over 1 April 2015 to 30 June 2017 study period for a lag of SM preceding EVI by 8 days. Shading in blue (red) color means DA_SMOPS has stronger (weaker) correlations with the MODIS-EVI. The gray color shading indicates insignificant differences. Patterns for DA_ASCATA and DA_ASCATB are very similar. DA = data assimilation; CTR = control run; OLP = open loop run; SMOPS = Soil Moisture Operational Product System; SMAP = Soil Moisture Active Passive; ASCAT = Advanced Scatterometer; SMOS = Soil Moisture and Ocean Salinity; AMSR = Advanced Microwave Scanning Radiometer for Earth Observing System.

40°N over both CTR and OLP runs. Distributions of the differences in Pearson correlations for the topsoil layer are only partly propagated to the deeper soil layers (Figures 9e and 9f), which lead to the largest improvements over the CTR and OLP cases decrease to 0.2 and 0.4, respectively. Besides, all of individual DA cases have better consistency with the MODIS-EVI for not only 10-cm but also 100-cm SM simulations in the north areas of 40°N in comparison with the CTR and OLP runs (Figure 11). Yet DA_AMSR performs similar with the OLP run in 60–80°N areas where the AMSR2 product has barely data availability (Figure 1).

5. Discussions

Results in section 4 indicate that there are remarkable differences in the data availability, time series average, and SD between the bias-corrected SMOPS and individual SM products, which result in significant distinctions in Noah LSM-based surface and root zone SM estimations between DA_SMOPS and each of five individual DA cases. With respect to the quality-controlled daily observations from the SCAN network and the 8-daily MODIS EVI products, the Noah LSM with benefits of assimilating the SMOPS SM data sets shows remarkable enhancements on 0- to 10-cm SM estimations with reducing RMSE values (Table 3; Figures 7 and 8) and raising correlation coefficients (Figures 10 and 11). However, this kind of positive information for the top surface soil layer is unsuccessfully propagated to the deeper soil layers (Table 3; Figure 11). Further considerations relevant to interpret the detection results are discussed in this section associated with model structure, DA characteristics, and complementary evaluations.

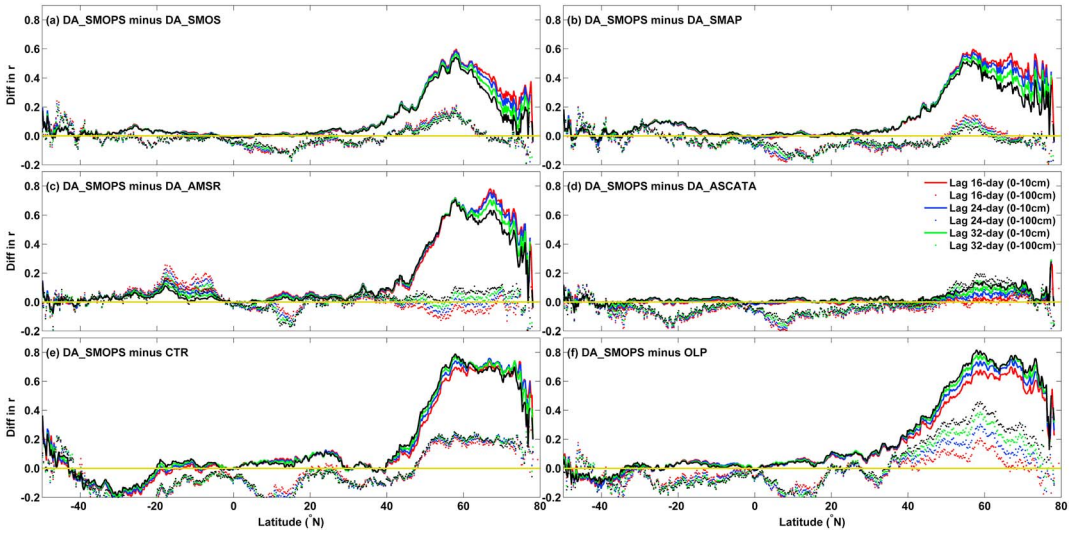

Figure 11. With respect to 8-daily MODIS EVI, zonal-averaged Pearson correlation (*r*) differences between DA_SMOPS and DA of each individual retrievals for lags of SM preceding EVI by 8 days (red), 16 days (blue), 24 days (green), and 32 days (black). The solid line indicates 0- to 10-cm SM simulations, while the dot line indicates the corresponding 0- to 100-cm SM simulations. The positive (negative) value indicates an improvement (degradation) with benefits of DA_SMOPS. The yellow line indicates the "0" position and over the yellow line DA_SMOPS performs better, whereas below the yellow line means degradation caused by DA_SMOPS. Patterns for DA_ASCATA and DA_ASCATB are very similar. DA = data assimilation; CTR = control run; OLP = open loop run; SMOPS = Soil Moisture Operational Product System; SMAP = Soil Moisture Active Passive; ASCAT = Advanced Scatterometer; SMOS = Soil Moisture and Ocean Salinity; AMSR = Advanced Microwave Scanning Radiometer for Earth Observing System.

5.1. Weights of Individual SM Retrievals in SMOPS Blended Product

All individual DA cases in this paper demonstrate good metrics to improve Noah model SM estimations for surface soil layer in comparison with the OLP run. Higher data availability of SM retrievals may thus lead to the corresponding DA case has better performance. With benefits of assimilating SMOPS SM that has the stable high data availability (Figures 1 and 2), improvements on 0- to 10-cm SM simulations are clearly shown with decreasing the SCAN observations-based RMSEs and raising correlations with respect to the MODIS-EVI data in comparison with the OLP run and each of the five individual DA cases.

Still a small amount of degradations are found when comparing the DA_SMOPS case with the OLP run. For instant, in Figure 7, DA_SMOPS presents a modest performance at couple sites scattering in the central-south CONUS, where DA_SMAP exhibits lower RMSE values over the DA_SMOPS. These degradations caused by assimilating SMOPS SM data are thus expected to be compensated for by objectively merging individual SM retrievals through increasing the weights of the SMAP product in the corresponding areas.

Besides, with respect to MODIS-EVI, DA_SMOPS shows negative correlations in east United States (Figure 9), which is expected to be improved by increasing weights of SMOS, SMAP, and ASCAT in SMOPS blended SM data (Figure 10). DA_SMOPS may present much stronger agreement with MODIS-EVI in west Europe with enhancing both SMOS and SMAP weighs in the area (Figures 9 and 10), while DA_SMOPS will show more successful performance in west United States and west Russia if AMSR2 and ASCAT weights can be raised in the corresponding areas, respectively.

However, the SMOPS SM data are currently developed using an equal-weight approach with subjectively combing all available individual SM retrievals under assumption of the relative importance of each quantity on the average. In this case, high- and poor-quality individual retrievals have equal opportunities to impact DA_SMOPS performance when they are all available. Supplementary improvements on SMOPS SM quality and in turn further enhancing DA_SMOPS performance are thus expected through increasing weight for high-quality individual SM retrieval and decreasing poor-quality retrieval weight in combination processing.

5.2. Model Hydrology

Compared to the OLP run, model SM estimations for the surface and root zone soil layers are significantly improved with benefits of both blended and individual SM retrievals. And relative to the individual DA

cases, the DA_SMOPS exhibits further improvements on 0- to 10-cm SM simulations with reducing the SCAN-based RMSE values and (Table 3; Figure 7) and strengthening the correlations with respect to the MODIS EVI data (Figures 9 and 10). Yet the behaviors of the topsoil layer SM simulations are not completely mirrored in the root zone SM estimations (Table 3; Figure 11) with DA_SMOPS showing slight degradations in comparison with the individual DA cases.

In fact, in a DA system, propagation of surface information to deeper soil layers mainly depends on the inherent surface-root zone connection of the LSM. Specifically, over four soil layers in the Noah LSM, the prognostic equations for the volumetric SM content depend on the soil water diffusivity and hydraulic conductivity (Chen & Dudhia, 2001; Ek et al., 2003) as

$$d_{z_1}\frac{\partial\theta_1}{\partial t} = -D\left(\frac{\partial\theta}{\partial z}\right)_{z_1} - K_{z_1} + P_d - R - E_{dir} - E_{t_1}, \tag{9}$$

$$d_{z_2}\frac{\partial\theta_2}{\partial t} = D\left(\frac{\partial\theta}{\partial z}\right)_{z_1} - D\left(\frac{\partial\theta}{\partial z}\right)_{z_2} + K_{z_1} - K_{z_2} - E_{t_2}, \tag{10}$$

$$d_{z_3}\frac{\partial\theta_3}{\partial t} = D\left(\frac{\partial\theta}{\partial z}\right)_{z_2} - D\left(\frac{\partial\theta}{\partial z}\right)_{z_3} + K_{z_2} - K_{z_3} - E_{t_3}, \tag{11}$$

$$d_{z_4}\frac{\partial\theta_4}{\partial t} = D\left(\frac{\partial\theta}{\partial z}\right)_{z_3} - D\left(\frac{\partial\theta}{\partial z}\right)_{z_4} + K_{z_{43}} - K_{z_4}, \tag{12}$$

where d_{z_i} is the ith soil layer thickness. P_d indicates the precipitation that is not intercepted by the canopy. E_{dir} and E_{ti} are the soil evaporation and the canopy transpiration taken by the canopy root in the ith soil layer, respectively. The surface runoff, R, is defined as the excess of precipitation not infiltrated into the soil. At the bottom of the soil model, the hydraulic diffusivity is assumed to be zero, so that the soil water flux is due only to the "gravitational" percolation term K_{z_4}, also named subsurface z_4 runoff or drainage.

Associated with equations (1)–(4) and (9)–(12), we can find that the soil water diffusivity in the Noah model is expressed for a rigid, isotropic, homogeneous, and one-dimensional vertical flow domain (Chen & Dudhia, 2001). However, SM distribution is affected by soil heterogeneity with spatial varying in texture, porosity, structure, and macroporosity (Crow et al., 2012). The hydraulic conductivity is largely nonlinear relying on the SM with sensitivity to SM fluctuations and soil properties (Cuenca et al., 1996). Yet the hydraulic conductivity associated with other soil variables is default defined in the Noah LSM as constants according to the soil texture map (Chen & Dudhia, 2001; Cosby et al., 1984; Ek et al., 2003), which indeed cannot provide optimal soil hydraulic properties (Kishné et al., 2017; Shellito et al., 2016). Besides, reasonable vertical soil hydrology in Noah model is also hampered by the layer soil texture used to represent the entire 2-m soil column (Xia et al., 2015). The heterogeneity of soil texture with depth will result in variations in the corresponding soil hydraulic properties, and in turn to unreasonable propagations of surface information to deeper soil layers (Peschel et al., 2006).

5.3. Perturbation Parameters

In the EnKF-based DA system, model states are generated by using perturbations for meteorological forcing parameters and state variables. In general, the implicit assumption is that adding mean-zero Gaussian noise to the forcing and state variables in the EnKF should not cause a systematic error in model output. Yet ongoing research indicates that degradations on model performance in deeper soil layers may be caused by the ensemble perturbations in SM states (Ryu et al., 2009). With narrowing this study to intercompare Noah LSM skills with benefits of assimilating blended and individual SM retrievals, the OLP run and each DA case were conducted under the unified perturbation conditions that are the same with LIS examples using Kumar et al. (2009), while previous study indicates that SM errors in deeper soil layers may be compensated for by correcting unintended perturbation biases (Ryu et al., 2009). Given good performance of Noah model SM simulations in surface soil layer with benefits of assimilating SMOPS blended SM data, it is thus expected to further reduce uncertainties of root-zone SM estimations using the optimal perturbation factors. However, how to optimize perturbations for each of the six DA cases (DA_SMOPS and five individual DA cases) is out the scope of this paper.

6. Conclusions

Noah LSM performance with benefits of assimilating a combination of the products from multiple sensors was intercompared with advances of assimilating individual SM retrievals. In situ observations-based RMSE and complementary evaluations using MODIS EVI products are conducted to measure the metrics from assimilating the SMOPS blended SM data sets. Three key results obtained in this paper are the following:

1. Relative to the individual SM retrievals, the SMOPS blended product (version 3.0) has much higher data availability. Specifically, data availability can be improved by the SMOPS blended product can reach to 70% and 50% in comparison with the passive and active SM retrievals, respectively.
2. After bias corrections of the six satellite SM retrievals to the climatology of Noah model-based 0- to 10-cm SM simulations using the CDF-matching method, SMOPS blended product shows drier patterns and lower temporal dynamics over SMOS and SMAP products. Relative to the ASCAT and the AMSR2 SM retrievals, however, SMOPS blended product illustrates significantly wetter patterns and larger SDs.
3. All of the DA cases show significant improvements on Noah model SM simulations for not only 0- to 10-cm soil layer but also root zone soil layer with reducing the SCAN observations-based RMSEs and raising the correlations with respect to the MODIS EVI data. And the Noah model with benefits of SMOPS blended SM product performs much better for the surface soil layer SM estimations over each of the five individual DA cases. However, this kind of positive information is not successfully propagated to deeper soil layer.

Acknowledgments
This work was supported by a grant from NOAA JPSS Proving Ground and Risk Reduction (PGRR) Program. We are also grateful to the anonymous reviewers for helping to significantly improve the quality of the manuscript. SMOPS soil moisture data product can be obtained from the NOAA NESDIS at http://www.ospo.noaa.gov/Products/land/smops/.

References

Albergel, C., Munier, S., Bocher, A., Bonan, B., Zheng, Y., Draper, C., et al. (2018). LDAS-Monde sequential assimilation of satellite derived observations applied to the contiguous US: An ERA-5 driven reanalysis of the land surface variables. *Remote Sensing*, *10*(10), 10. https://doi.org/10.3390/rs10101627

Bolten, J. D., & Crow, W. T. (2012). Improved prediction of quasi-global vegetation conditions using remotely-sensed surface soil moisture. *Geophysical Research Letters*, *39*, L19406. https://doi.org/10.1029/2012GL053470

Brocca, L., Crow, W. T., Ciabatta, L., Massari, C., De Rosnay, P., Enenkel, M., et al. (2017). A review of the applications of ASCAT soil moisture products. *IEEE Journal of Selected Topics in Applied Earth Observations and Remote Sensing*, *10*, 2285–2306.

Chen, F., & Dudhia, J. (2001). Coupling an advanced land surface-hydrology model with the Penn State–NCAR MM5 modeling system. Part I: Model implementation and sensitivity. *Monthly Weather Review*, *129*(4), 569–585. https://doi.org/10.1175/1520-0493(2001)129<0569:CAALSH>2.0.CO;2

Colliander, A., Jackson, T. J., Bindlish, R., Chan, S., Das, N., Kim, S. B., et al. (2017). Validation of SMAP surface soil moisture products with core validation sites. *Remote Sensing of Environment*, *191*, 215–231. https://doi.org/10.1016/j.rse.2017.01.021

Cosby, B. J., Hornberger, G. M., Clapp, R. B., & Ginn, T. R. (1984). A statistical exploration of the relationships of soil moisture characteristics to the physical properties of soils. *Water Resources Research*, *20*(6), 682–690.

Crow, W. T., Kumar, S. V., & Bolten, J. D. (2012). On the utility of land surface models for agricultural drought monitoring. *Hydrology and Earth System Sciences*, *16*, 3451–3460.

Crow, W. T., & Wood, E. F. (2003). The assimilation of remotely sensed soil brightness temperature imagery into a land surface model using ensemble Kalman filtering: A case study based on ESTAR measurements during SGP97. *Advances in Water Resources*, *26*, 137–149.

Cuenca, R. H., Ek, M., & Mahrt, L. (1996). Impact of soil water property parameterization on atmospheric boundary-layer simulation. *Journal of Geophysical Research*, *101*(D3), 7269–7277. https://doi.org/10.1029/95JD02413

Dharssi, I., Bovis, K., Macpherson, B., & Jones, C. (2011). Operational assimilation of ASCAT surface soil wetness at the met Office. *Hydrology and Earth System Sciences*, *15*(8), 2729–2746. https://doi.org/10.5194/hess-15-2729-2011

Dorigo, W., Wagner, W., Albergel, C., Albrecht, F., Balsamo, G., Brocca, L., et al. (2017). ESA CCI soil moisture for improved Earth system understanding: State-of-the art and future directions. *Remote Sensing of Environment*, *203*, 186–215.

Draper, C. S., Reichle, R. H., De Lannoy, G. J., & Liu, Q. (2012). Assimilation of passive and active microwave soil moisture retrievals. *Geophysical Research Letters*, *39*, L04401. https://doi.org/10.1029/2011GL050655

Ek, M. B., Mitchell, K. E., Lin, Y., Rogers, E., Grunmann, P., Koren, V., et al. (2003). Implementation of Noah land surface model advances in the National Centers for Environmental Prediction operational mesoscale Eta model. *Journal of Geophysical Research*, *108*(D22), 8851. https://doi.org/10.1029/2002JD003296

Entekhabi, D., Njoku, E. G., O'Neill, P. E., Kellogg, K. H., Crow, W. T., Edelstein, W. N., et al. (2010). The Soil Moisture Active Passive (SMAP) mission. *Proceedings of the IEEE*, *98*(5), 704–716. https://doi.org/10.1109/JPROC.2010.2043918

Evensen, G. (1994). Sequential data assimilation with a nonlinear quasi-geostrophic model using Monte Carlo methods to forecast error statistics. *Journal of Geophysical Research*, *99*(C5), 10,143–10,162. https://doi.org/10.1029/94JC00572

JAXA (2013). Descriptions of GCOM-W1 AMSR2 level 1R and level 2 algorithms. NDX-120015A, Jul. 9

Jiang, Z., Huete, A. R., Didan, K., & Miura, T. (2008). Development of a two-band enhanced vegetation index without a blue band. *Remote Sensing of Environment*, *112*, 3833–3845.

Kerr, Y. H., Waldteufel, P., Wigneron, J.-P., Delwart, S., Cabot, F., Boutin, J., et al. (2010). The SMOS mission: New tool for monitoring key elements of the globalwater cycle. *Proceedings of the IEEE*, *98*(5), 666–687. https://doi.org/10.1109/JPROC.2010.2043032

Kishné, A., Yimam, Y. T., Morgan, C. L. S., & Dornblaser, B. C. (2017). Evaluation and improvement of the default soil hydraulic parameters for the Noah Land Surface Model. *Geoderma*, *285*, 247–259. https://doi.org/10.1016/j.geoderma.2016.09.022

Kolassa, J., Reichle, R. H., & Draper, C. S. (2017). Merging active and passive microwave observations in soil moisture data assimilation. *Remote Sensing of Environment*, *191*, 117–130.

Koster, R. D., Dirmeyer, P. A., Guo, Z., Bonan, G., Chan, E., Cox, P., et al. (2004). Regions of strong coupling between soil moisture and precipitation. *Science*, *305*(5687), 1138–1140. https://doi.org/10.1126/science.1100217

Koster, R. D., Guo, Z., Yang, R., Dirmeyer, P. A., Mitchell, K., & Puma, M. J. (2009). On the nature of soil moisture in land surface models. *Journal of Climate*, *22*(16), 4322–4335. https://doi.org/10.1175/2009JCLI2832.1

Kumar, S. V., Reichle, R. H., Koster, R. D., Crow, W. T., & Peters-Lidard, C. D. (2009). Role of subsurface physics in the assimilation of surface soil moisture observations. *Journal of Hydrometeorology*, *10*(6), 1534–1547. https://doi.org/10.1175/2009JHM1134.1

Leroux, D. J., Calvet, J.-C., Munier, S., & Albergel, C. (2018). Using satellite-derived vegetation products to evaluate LDAS-Monde over the Euro-Mediterranean area. *Remote Sensing*, *10*(8), 1199. https://doi.org/10.3390/rs10081199

Li, B., Toll, D., Zhan, X., & Cosgrove, B. (2012). Improving estimated soil moisture fields through assimilation of AMSR-E soil moisture retrievals with an ensemble Kalman filter and a mass conservation constraint. *Hydrology and Earth System Sciences*, *16*, 105–119.

Li, L., Gaiser, P. W., Gao, B.-C., Bevilacqua, R. M., Jackson, T. J., Njoku, E. G., et al. (2010). WindSat global soil moisture retrieval and validation. *IEEE Transactions on Geoscience and Remote Sensing*, *48*(5), 2224–2241.

Lievens, H., Tomer, S. K., al Bitar, A., de Lannoy, G. J. M., Drusch, M., Dumedah, G., et al. (2015). SMOS soil moisture assimilation for improved hydrologic simulation in the Murray Darling Basin, Australia. *Remote Sensing of Environment*, *168*, 146–162. https://doi.org/10.1016/j.rse.2015.06.025

Liu, J., Zhan, X., Hain, C., Yin, J., Fang, L., Li, Z., & Zhao, L. (2016). *NOAA Soil Moisture Operational Product System (SMOPS) and its validations* (pp. 3477–3480). Beijing, China: IEEE Geoscience and Remote Sensing Symposium (IGARSS).

Liu, Q., Reichle, R. H., Bindlish, R., Cosh, M. H., Crow, W. T., de Jeu, R., et al. (2011). The contributions of precipitation and soil moisture observations to the skill of soil moisture estimates in a land data assimilation system. *Journal of Hydrometeorology*, *12*(5), 750–765. https://doi.org/10.1175/JHM-D-10-05000.1

Maeda, T., Taniguchi, Y., & Imaoka, K. (2016). GCOM-W1 AMSR2 level 1R product: Dataset of brightness temperature modified using the antenna pattern matching technique. *IEEE Transactions on Geoscience and Remote Sensing*, *54*(2), 770–782.

Mazrooei, A., Sinha, T., Sankarasubramanian, A., Kumar, S., & Peters-Lidard, C. D. (2015). Decomposition of sources of errors in seasonal streamflow forecasting over the U.S. Sunbelt. *Journal of Geophysical Research: Atmospheres*, *120*, 11,809–11,825. https://doi.org/10.1002/2015JD023687

Nair, A. S., & Indu, J. (2016). Enhancing Noah land surface model prediction skill over Indian Subcontinent by assimilating SMOPS blended soil moisture. *Remote Sensing*, *8*(12), 976. https://doi.org/10.3390/rs8120976

Njoku, E. G., Jackson, T. J., Lakshmi, V., Chan, T. K., & Nghiem, S. V. (2003). Soil moisture retrieval from AMSR-E. *IEEE Transactions on Geoscience and Remote Sensing*, *41*(2), 215–229. https://doi.org/10.1109/TGRS.2002.808243

Peschel, J. M., Haan, P. K., & Lacey, R. E. (2006). Influences of soil data set resolution on hydrologic modeling. *Journal of the American Water Resources Association*, *42*, 1371–1389.

Peters-Lidard, C. D., Mocko, D. M., Garcia, M., Santanello, J. A. Jr., Tischler, M. A., Moran, M. S., & Wu, Y. (2008). Role of precipitation uncertainty in the estimation of hydrologic soil properties using remotely sensed soil moisture in a semi-arid environment. *Water Resources Research*, *44*, W05S18. https://doi.org/10.1029/2007WR005884

Reichle, R. H., De Lannoy, G. J., Liu, Q., Ardizzone, J. V., Colliander, A., Conaty, A., et al. (2017). Assessment of the SMAP level-4 surface and root-zone soil moisture product using in situ measurements. *Journal of Hydrometeorology*, *18*(10), 2621–2645. https://doi.org/10.1175/JHM-D-17-0063.1

Reichle, R. H., & Koster, R. D. (2004). Bias reduction in short records of satellite soil moisture. *Geophysical Research Letters*, *31*, L19501. https://doi.org/10.1029/2004GL020938

Richards, L. A. (1931). Capillary conduction of liquids in porous mediums. *Physics*, *1*(5), 318–333. https://doi.org/10.1063/1.1745010

Robinson, D. A., Campbell, C. S., Hopmans, J. W., Hornbuckle, B. K., Jones, S. B., Knight, R., et al. (2008). Soil moisture measurements for ecological and hydrological watershed scale observatories: A review. *Vadose Zone Journal*, *7*(1), 358–389. https://doi.org/10.2136/vzj2007.0143

Rodell, M., Houser, P. R., Jambor, U., Gottschalck, J., Mitchell, K., Meng, C. J., et al. (2004). The Global Land Data Assimilation System. *Bulletin of the American Meteorological Society*, *85*(3), 381–394. https://doi.org/10.1175/BAMS-85-3-381

Rodriguez-Iturbe, I., D'Odorico, P., Porporato, A., & Ridolfi, L. (1999). On the spatial and temporal links between vegetation, climate, and soil moisture. *Water Resources Research*, *35*, 3709–3722.

Ryu, D., Crow, W. T., Zhan, X., & Jackson, T. J. (2009). Correcting unintended perturbation biases in hydrologic data assimilation. *Journal of Hydrometeorology*, *10*(3), 734–750. https://doi.org/10.1175/2008JHM1038.1

Sawada, Y. (2018). Quantifying drought propagation from soil moisture to vegetation dynamics using a newly developed ecohydrological land reanalysis. *Remote Sensing*, *10*(8), 1197. https://doi.org/10.3390/rs10081197

Schaefer, G. L., Cosh, M. H., & Jackson, T. J. (2007). The USDA Natural Resources Conservation Service Soil Climate Analysis Network (SCAN). *Journal of Atmospheric and Oceanic Technology*, *24*(12), 2073–2077. https://doi.org/10.1175/2007JTECHA930.1

Schwinning, S., Sala, O. E., Loik, M. E., & Ehleringer, J. R. (2004). Thresholds, memory, and seasonality: Understanding pulse dynamics in arid/semi-arid ecosystems. *Oecologia*, *141*(2), 191–193. https://doi.org/10.1007/s00442-004-1683-3

Seneviratne, S. I., Corti, T., Davin, L. E., Hirschi, M., Jaeger, E. B., Lehner, I., et al. (2010). Investigating soil moisture–climate interactions in a changing climate: A review. *Earth-Science Reviews*, *99*, 125–161.

Shellito, P. J., Small, E. E., & Cosh, M. H. (2016). Calibration of Noah soil hydraulic property parameters using surface soil moisture from SMOS and basin wide in situ observations. *Journal of Hydrometeorology*, *17*(8), 2275–2292. https://doi.org/10.1175/JHM-D-15-0153.1

Turcu, V. E., Jones, S. B., & Or, D. (2005). Continuous soil carbon dioxide and oxygen measurements and estimation of gradient-based gaseous flux. *Vadose Zone Journal*, *4*, 1161–1169.

van der Schrier, G., & Barkmeijer, J. (2007). North American 1818–1824 drought and 1825–1840 pluvial and their possible relation to the atmospheric circulation. *Journal of Geophysical Research*, *112*, D13102. https://doi.org/10.1029/2007JD008429

Wagner, W., Hahn, S., Kidd, R., Melzer, T., Bartalis, Z., Hasenauer, S., et al. (2013). The ASCAT soil moisture product: A review of its specifications, validation results, and merging applications. *Meteorologische Zeitschrift*, *22*(1), 5–33. https://doi.org/10.1127/0941-2948/2013/0399

Walker, J. P., & Houser, P. R. (2001). A methodology for initializing soil moisture in a global climate model: Assimilation of near-surface soil moisture observations. *Journal of Geophysical Research*, *106*(D11), 11,761–11,774.

Xia, Y., Ek, M. B., Wu, Y., Ford, T. W., & Quiring, S. M. (2015). Comparison of NLDAS-2 simulated and NASMD observed daily soil moisture. Part II: Impact of soil texture classification and vegetation type mismatches. *Journal of Hydrometeorology*, *16*, 1981–2000.

Xia, Y., Mitchell, K., Ek, M., Sheffield, J., Cosgrove, B., Wood, E., et al. (2012). Continental-scale water and energy flux analysis and validation for the North American Land Data Assimilation System project phase 2 (NLDAS-2): 1. Intercomparison and application of model products. *Journal of Geophysical Research*, *117*, D03109. https://doi.org/10.1029/2011JD016048

Yin, J., & Zhan, X. (2018). Impact of bias-correction methods on effectiveness of assimilating SMAP soil moisture data into NCEP global forecast system using the ensemble Kalman filter. *IEEE Geoscience and Remote Sensing Letters*, *15*(5), 659–663. https://doi.org/10.1109/LGRS.2018.2806092

Yin, J., Zhan, X., Zheng, Y., Hain, C., Liu, J., & Fang, L. (2015). Optimal ensemble size of Ensemble Kalman Filter in sequential soil moisture data assimilation of land surface model. *Geophysical Research Letters*, *16*, 6710–6715. https://doi.org/10.1002/2015GL063366

Yin, J., Zhan, X., Zheng, Y., Liu, J., Fang, L., & Hain, C. R. (2015). Enhancing model skill by assimilating SMOPS blended soil moisture product into Noah land surface model. *Journal of Hydrometeorology*, *16*(2), 917–931. https://doi.org/10.1175/JHM-D-14-0070.1

Yin, J., Zhan, X., Zheng, Y., Liu, J., Hain, C. R., & Fang, L. (2014). impact of quality control of satellite soil moisture data on their assimilation into land surface model. *Geophysical Research Letters*, *41*, 7159–7166. https://doi.org/10.1002/2014GL060659

Yin, J., Zheng, Y., Zhan, X., Hain, C. R., Zhai, Q., Duan, C., et al. (2015). An assessment of impacts of surface type changes on drought monitoring. *International Journal of Remote Sensing*, *36*(24), 6116–6134. https://doi.org/10.1080/01431161.2015.1111539